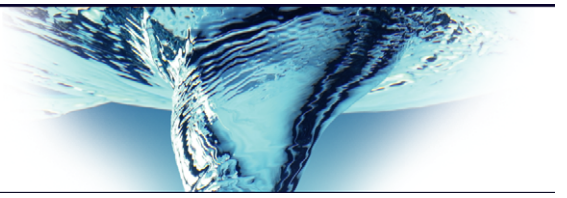
JFM RAPIDS
journals.cambridge.org/rapids



The Richtmyer–Meshkov instability of a three-dimensional air/SF_6 interface with a minimum-surface feature

Xisheng Luo†, Xiansheng Wang and Ting Si

Advanced Propulsion Laboratory, Department of Modern Mechanics, University of Science and Technology of China, Hefei 230026, China

(Received 31 January 2013; revised 5 March 2013; accepted 8 March 2013;
first published online 4 April 2013)

A novel method to create a discontinuous gaseous interface with a minimum-surface feature by the soap film technique is developed for three-dimensional (3D) Richtmyer–Meshkov instability (RMI) studies. The interface formed is free of supporting mesh and the initial condition can be well controlled. Five air/SF_6 interfaces with different amplitude are realized in shock-tube experiments. Time-resolved schlieren and planar Mie-scattering photography are employed to capture the motion of the shocked interface. It is found that the instability at the linear stage in the symmetry plane grows much slower than the predictions of previous two-dimensional (2D) impulsive models, which is ascribed to the opposite principal curvatures of the minimum surface. The 2D impulsive model is extended to describe the general 3D RMI. A quantitative analysis reveals a good agreement between experiments and the extended linear model for all the configurations including both the 2D and 3D RMIs at their early stages. An empirical model that combines the early linear growth with the late-time nonlinear growth is also proposed for the whole evolution process of the present configuration.

Key words: compressible turbulence, nonlinear instability, shock waves

1. Introduction

The Richtmyer–Meshkov instability (RMI) occurs when an initially perturbed interface between two fluids with different density is impulsively accelerated (Richtmyer 1960; Meshkov 1969). The growth of perturbations generally intensifies the mixing between the fluids and eventually induces turbulence in the flow. This hydrodynamic instability has become increasingly attractive to researchers owing to its

† Email address for correspondence: xluo@ustc.edu.cn

 © Cambridge University Press 2013
doi:10.1017/jfm.2013.148

https://doi.org/10.1017/jfm.2013.148 Published online by Cambridge University Press

significant applications in many fields (Ranjan, Oakley & Bonazza 2011) such as inertial confinement fusion (ICF) and supernova explosions.

The first consideration of the RMI was introduced theoretically by Richtmyer (1960) and an impulsive model was proposed using a two-dimensional (2D) linear stability analysis. The result was then confirmed experimentally by Meshkov (1969). The 2D impulsive model is found to be applicable at the early linear stage of evolution (Collins & Jacobs 2002). However, when the nonlinearity becomes significant in the flow, a great discrepancy is found between the theoretical predictions and experimental results (Rikanati *et al.* 2003). To capture the growth of the instability from the early linear stage to the late-time nonlinear stage, several models have been developed and agreement obtained among the experiments, theories and simulations (Sadot *et al.* 1998; Zabusky 1999; Oron *et al.* 2001; Brouillette 2002; Ranjan *et al.* 2011). Most of these studies focused on the 2D RMI because of its simple configuration. Recently, the three-dimensional (3D) RMI has received much attention due to its more practical nature. A few 3D configurations such as the 3D single-mode and the random-perturbed cases have been considered experimentally and theoretically (Zhang & Sohn 1999; Yosef-Hai *et al.* 2003; Chapman & Jacobs 2006; Leinov *et al.* 2009; Long *et al.* 2009). However, there is a scarcity of 3D RMI experimental studies. A great challenge to such experimental studies is to form a well-defined initial interface, which motivates the present work.

Most previous experimental studies were performed in shock tube environments with a continuous or discontinuous interface. Techniques to form a continuous interface, such as the gas cylinder and gas curtain, are often employed to avoid the influences of membrane and support (Brouillette 2002). However, the exact initial conditions such as the distribution of the gas concentration and the small vertical velocity of the gas curtain have to be determined afterwards, and their effects on the instability are still unclear. A nitrocellulosic membrane is usually employed to form a quasi-sinusoidal sharp interface (Meshkov 1969; Mariani *et al.* 2008). Due to the absorption of the fluid kinetic energy, the remaining membrane pieces are found to be influential in the late-time evolution. It is also hard to obtain the exact shape of initial perturbations in the experiment. Therefore, approximate initial conditions have been employed in the past numerical attempts, and the wire mesh supports are often simply neglected. Another method to form the discontinuous interface is the soap film technique often used in shock–bubble interaction (Ranjan *et al.* 2011). Good agreement is obtained among the experiments, simulations and theories (Haas & Sturtevant 1987; Layes, Jourdan & Houas 2009; Ranjan *et al.* 2011; Zhai *et al.* 2011; Si *et al.* 2012). It is indicated that the soap droplets after the shock impact could absorb less energy from the fluids. However, a soap film is seldom used to form a density interface other than the spherical or cylindrical bubble mainly due to the difficulty in controlling its shape. Recently a new method to form polygonal soap film interfaces has been developed by using thin pins around polygonal vertexes (Wang, Si & Luo 2013).

In the present study, a novel method to create a discontinuous gaseous interface with a minimum-surface feature is developed by the soap film technique for a 3D RMI study. The interface formed is free of supporting mesh or pins and, therefore, the initial condition can be well controlled. Owing to the minimum-surface feature, this interface has a zero mean curvature, which is different from the interface used in the previous literature (Yosef-Hai *et al.* 2003; Chapman & Jacobs 2006; Long *et al.* 2009). Krechetnikov (2009) theoretically studied the effect of interface curvature on the RMI and pointed out that in the 3D case there are some open questions, in particular the stability characteristics of a surface curved in the transverse and the longitudinal

https://doi.org/10.1017/jfm.2013.148 Published online by Cambridge University Press

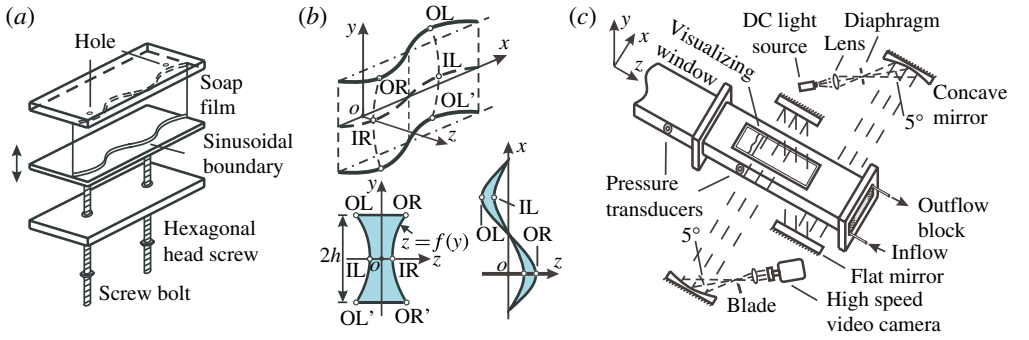


FIGURE 1. (*a*) Schematic of the device to generate the soap film interface. (*b*) The interface formed in a 3D view (upper), top view (lower-left) and side view (lower-right) with IL, IR, IL' and OL, OR, OR' (I, inner; O, outer; L, left; R, right) denoting the positions of the crests and troughs of the perturbed interface at $z = 0$ and $\pm h$, respectively. (*c*) The test section of the shock tube with the schlieren system.

directions are not understood yet. Understanding the curvature effect in the 3D RMI is another purpose of this study.

2. Experimental methods

2.1. *Formation and feature of the initial interface*

The device to generate the initially perturbed interface is sketched in figure 1(*a*), and it mainly consists of two fixed acrylic sheets, a movable acrylic sheet between them, and two sinusoidal wires. On the upper fixed sheet and the movable sheet, matching sinusoidal channels are engraved in which to mount the wires so that they touch. The two fixed acrylic sheets are stuck tightly to the visualizing windows as shown in figure 1(*c*). The movable sheet is first raised up so that the wires, embedded in the movable sheet and the upper fixed sheet, contact with each other tightly. Then, the soap liquid (made of 78 % distilled water, 2 % sodium oleate and 20 % glycerine by mass) is injected into the channel through the holes (∼1.5 mm in diameter) in the upper fixed sheet. When both wires are wetted completely, the movable sheet is pulled down slowly toward the lower fixed sheet and the soap film interface is generated. Finally, the screws are tightened to avoid leakage of the test gas.

The boundary of the soap film is determined by the sinusoidal wires and the interface formed is free of mesh and support. Therefore, the shape of the initially perturbed interface can be well controlled in each experiment as depicted in figure 1(*b*). Because the gas on both sides of the interface is at ambient pressure, the soap film interface formed has a zero mean curvature and the geometry can be characterized as minimum surface (Isenberg 1992). The interface has a 3D configuration and two principal curvatures at every point of the interface are opposite.

The sinusoidal boundary across the span of the test section at $y = \pm h$ can be described as $z = a_o^0 \cos(kx)$ with a_o^0 the initial amplitude at the sinusoidal boundary, h the half-height of the test section and k the wavenumber defined as $k = 2\pi/\lambda$ with λ the wavelength.

https://doi.org/10.1017/jfm.2013.148 Published online by Cambridge University Press

The interface is single-mode in each y-plane because of the sinusoidal boundary and the interfacial geometry can be characterized as

$$z = f(y)\cos(kx), \quad y \in [-h, h]. \tag{2.1}$$

Based on the property of minimum surface (Isenberg 1992), the function $f(y)$ satisfies

$$f'' = k^2 f(1 + f'^2), \quad f'|_{y=0} = 0, \quad f|_{y=0} = a_i^0, \tag{2.2}$$

where a_i^0 is the perturbation amplitude of the symmetry plane $y = 0$. An expression derived from (2.2) is

$$y = \pm \int_{a_i^0}^{f(y)} \frac{\mathrm{d}x}{\sqrt{\exp\left[k^2[x^2 - (a_i^0)^2]\right] - 1}} \tag{2.3}$$

with the plus (minus) sign for $y > 0$ ($y < 0$). Considering the boundary condition $f|_{y=\pm h} = a_o^0$, the interfacial amplitude a_i^0 can be determined from (2.3), which has been confirmed by the experimental measurements with different sinusoidal boundaries.

2.2. *Shock-tube facility and diagnostics*

Experiments are conducted in a horizontal shock tube, which consists of a 1.7 m driver section, a 2.0 m driven section and a 0.6 m test section with a cross-section area of 140 mm × 20 mm. The height of the test section is small ($2h = 20$ mm) to minimize the gravity effect of the test gas and to generate an appropriate initial amplitude of the symmetry plane (a_i^0 is strongly dependent on the height of the shock tube, for instance, $a_i^0 = 0.175$ mm when $2h = 40$ mm and $a_o^0 = 3$ mm). The Mach number of the shock wave is 1.21 ± 0.01. Figure 1(*c*) presents a schematic of the test section. Two pressure transducers are mounted in the sidewall to provide the trigger signal for the recording system. The heavy test gas flows into the test section from the 'inflow' pipe and out from the 'outflow' pipe (diameter of pipes is 4 mm). An oxygen detector, located at the mouth of the 'outflow' pipe, is used to monitor the purity of gas in the test section.

A high-speed video camera (FASTCAM SA5, Photron Limited) is employed to record the interface evolution with two recording systems. One is schlieren photography (Zhai *et al.* 2011; Si *et al.* 2012) as shown in figure 1(*c*). The frame rate is 5×10^4 f.p.s. with a shutter time of 2 μs, which corresponds to a spatial resolution of ∼3.1 pixels mm^{-1}. The other recording system is planar Mie-scattering photography. The laser sheet, provided by a continuous laser (SDL-532-15000T, 15 W, 532 nm), is located in the symmetry plane of the initial interface. A quartz glass embedded in endwall of the test section allows the laser sheet to illuminate the observing region. Soap droplets from the soap film breakup are illuminated and employed as tracing particles. The frame rate is 3×10^4 f.p.s. with a shutter time of 4 μs, which corresponds to a spatial resolution of ∼4.5 pixels mm^{-1}.

3. Experimental results

Five interfaces with different amplitude are realized in the shock-tube experiments. The interfaces formed are periodic with a fixed wavelength of $\lambda = 35$ mm. The initial amplitude a_o^0 of the boundary varies from 3, 4, 5, 6 to 7 mm. Owing to the 3D feature of the interface, the amplitude a_i^0 of the symmetry plane is smaller than a_o^0. Specific values of these initial conditions are provided in table 1. Figure 2 shows schlieren sequences of the distorted interface in the experiments. The initial time corresponds to the instant when the incident shock wave passes $z = 0$.

https://doi.org/10.1017/jfm.2013.148 Published online by Cambridge University Press

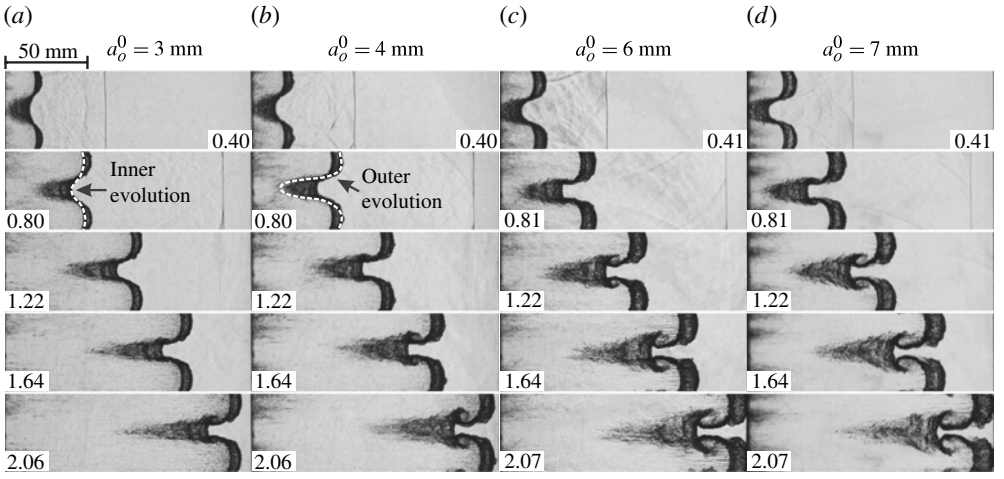


FIGURE 2. Schlieren sequences showing the evolution of shocked air(left)/SF_6(right) interface for initial amplitudes varying from 3 to 7 mm. The shock propagates from left to right. Inserted numbers indicate the time in ms.

a_o^0 (mm)	a_i^0 (mm)	λ (mm)	Ms	A^-	A^+	Z_c	v_i^{RM} (m s^{-1})
3	1.01	35	1.21	0.67	0.72	0.83	7.76
4	1.35	35	1.21	0.67	0.72	0.83	10.40
5	1.72	35	1.21	0.67	0.72	0.83	13.19
6	2.00	35	1.21	0.67	0.72	0.83	15.31
7	2.29	35	1.21	0.67	0.72	0.83	17.55

TABLE 1. Specific values of initial conditions in experiments. a_o^0 and a_i^0: initial amplitudes of the boundary plane and symmetry plane, respectively. λ: the initial wavelength. Ms: the incident shock Mach number. A: the Atwood number with superscript $-$ and $+$ denoting the pre- and post-shock quantities, respectively. Z_c: the compressible factor. v_i^{RM}: the initial growth rate predicted by the 2D impulsive model (equation (3.1)).

Owing to the 3D characteristic, the evolving interface in each y-plane behaves differently. In the present study, only the symmetry and boundary planes are considered. The interfacial evolution of the symmetry plane can be revealed by the inner contour in each image, as represented by the dashed line in figure 2, which has been confirmed by the planar Mie-scattering images. Figure 3(*a*) compares the experimental images obtained from the schlieren and the planar Mie-scattering photography for the same initial amplitude $a_o^0 = 6$ mm. The Mie-scattering images have been reversed so that the black contour represents the interface in the symmetry plane illuminated by the laser sheet. A good agreement on the inner evolution is found between the two sequences. It is also indicted that the inner evolution shows good symmetry at the early stage. As the instability grows, the interface becomes asymmetric when the structures of the bubble, spike and vortex dominate the flow. Figure 3(*b*) compares the evolution of the two sequences quantitatively. The growth of the symmetry plane, which is defined as the half-width of the interface in the

https://doi.org/10.1017/jfm.2013.148 Published online by Cambridge University Press

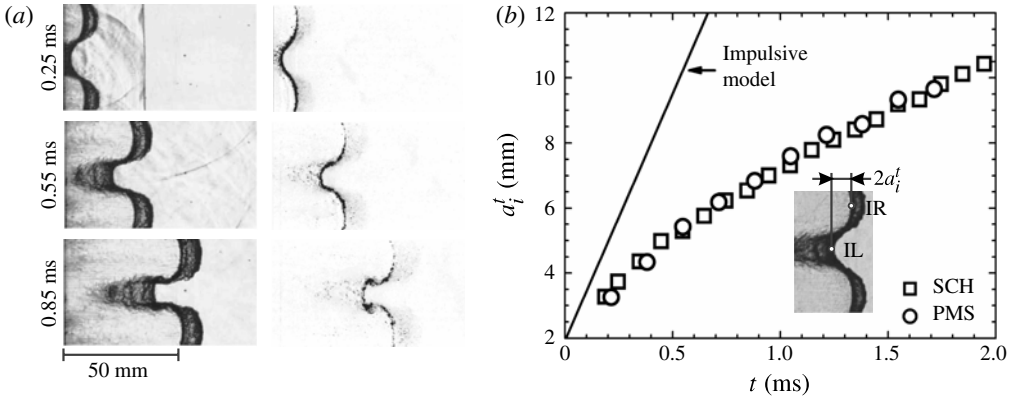


FIGURE 3. (*a*) Comparison of schlieren sequence (left) with planar Mie-scattering (right) photography. The initial amplitude a_o^0 is 6 mm and the time is indicated in ms. (*b*) Comparison of the amplitude a_i^t obtained from the schlieren (SCH) with the planar Mie-scattering (PMS) photography and the impulsive model (3.1).

symmetry plane, can be described by $a_i^t = (a_{ib}^t + a_{is}^t)/2$, with a_{ib}^t and a_{is}^t denoting the amplitudes of the evolving bubble and spike, respectively. The growth rate at the early stage can be estimated from the 2D impulsive model (Richtmyer 1960) as

$$v_i^{RM} = kZ_c a_i^0 A^+ \Delta v, \tag{3.1}$$

where the compression ratio is $Z_c = 1 - \Delta v/W_s$ (Meshkov 1969) with W_s the incident shock velocity and Δv the velocity jump of the shocked interface; the post-shock Atwood number $A^+ = (\rho_2 - \rho_1)/(\rho_2 + \rho_1)$ with ρ_1 and ρ_2 the post-shock densities of the air and SF_6, respectively. The specific values of these parameters are also listed in table 1. In the 2D case, the impulsive model is valid at early stages (e.g. $kv_0t < 0.7$) when the shock strength and the interfacial amplitude are small enough (Niederhaus & Jacobs 2003). However, in the present 3D case, the impulsive model over-predicts the instability growth as shown in figure 3(*b*). The pressure gradient (Brouillette 2002) and the baroclinic vorticity are assumed to be the driving mechanisms that account for the slower growth.

In the minimum-surface case, the pressure gradient at point IL/IR, induced by the reflected and transmitted waves in the horizontal (xz) plane, is from left to right as shown in figure 4(*a*), which will intensify the instability growth similarly to the 2D case. However, the pressure gradient induced by waves in the vertical (yz) plane is from right to left. Therefore, the growth of perturbations tends to be suppressed by this opposite pressure gradient. The RMI is mainly driven by the baroclinic vorticity created on the interface, due to the misalignment of density and pressure gradients (i.e. $\nabla\rho \times \nabla p \neq 0$). As illustrated in figure 4(*b*), the baroclinic vorticity along the sinusoidal line (IR–IL) enhances the instability, while that along the catenary line (OR–IR–OR' or OL–IL–OL') prevents its growth. It should be noted that in the 3D single-mode RMI (Chapman & Jacobs 2006; Long *et al.* 2009), where the principal curvatures at the crest or trough of the interface are in the same direction, the induced pressure gradients are in the same direction and, therefore, intensify the instability growth. So does the baroclinic vorticity in the 3D single-mode RMI. These findings confirmed the theoretical assertion of Krechetnikov (2009) on the curvature effect.

https://doi.org/10.1017/jfm.2013.148 Published online by Cambridge University Press

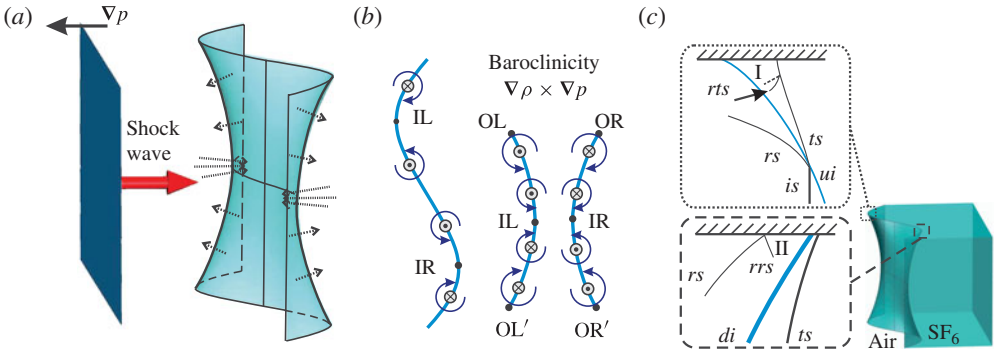


FIGURE 4. (*a*) The induced pressure gradients shown for the catenary lines OL–OL' and OR–OR'; (*b*) the baroclinic vorticity distribution; and (*c*) wave configurations at the boundaries: *is*, incident shock wave; *i*, initial interface; *ts*, transmitted shock; *rs*, reflected shock; *rts*, reflected transmitted shock.

In the present observations, the interfacial evolution of the symmetry plane is dependent on the initial condition. Like the same trend discovered in the 2D experiments (Niederhaus & Jacobs 2003), the interface evolves more quickly into asymmetry as the initial amplitude increases. The vortex also develops more quickly, which can be seen in the late-time evolution as shown in figure 3. The reason is that, as the initial amplitude becomes larger, more vorticity is created on the interface not only in the 2D single-mode case (Rikanati *et al.* 2003) but also in the present 3D configuration. The stronger vorticity drives the instability to grow faster.

The evolution of the interface in the boundary planes ($y = \pm h$) is revealed by the outer contour in each image, as marked by the dashed line in figure 2. In the outer evolution, the shocked interface on the boundary exhibits strong asymmetry, e.g. 0.4 ms in figure 2. After the shock impact, a distinct jet, which is induced by the reflection of the transmitted shock (*ts*), appears at the upstream interface (*ui*). The wave system at the corner between the boundary crest/trough and the wall is sketched in figure 4(*c*). When the shock wave impacts the *ui* in the boundary plane, i.e. OL in figure 1(*b*), the *ts* moves slower than the incident shock and therefore propagates toward the solid wall. The *ts* is reflected and a new shock wave (*rts*) appears between the *ts* and the *ui*. Note that the pressure behind the *rts* is much higher than that at the *ui*, and, driven by the higher pressure, an upstream-running jet is formed. At the late stage of the evolution, the jet flow becomes turbulent, as shown at 2.07 ms for $a_o = 7$ mm in figure 2. The downstream interface (*di*) in the boundary plane moves faster than that in the symmetry plane. The crescent structure, composed of the *di* in each plane, grows larger as the instability evolves. When the shock wave passes the *di* in the boundary plane, i.e. OR in figure 1(*b*), the reflected shock (*rs*) propagates toward the wall. Therefore, the *rs*, which is first reflected by the air/SF_6 interface, is secondly reflected by the wall. The high pressure behind this new reflected shock drives the *di* in the boundary plane, which results in a faster movement of the *di* in the boundary plane than in the symmetry plane. Therefore, the outer evolution appears quite asymmetric even at the very early stage. However, because the *rs* is much weaker than the *ts*, the induced high pressure is much smaller at the *di* than that at the *ui* and, therefore, no jet is observed at the *di*. The evolution of the interface in the boundary planes is also dependent on the initial condition. The larger the initial

https://doi.org/10.1017/jfm.2013.148 Published online by Cambridge University Press

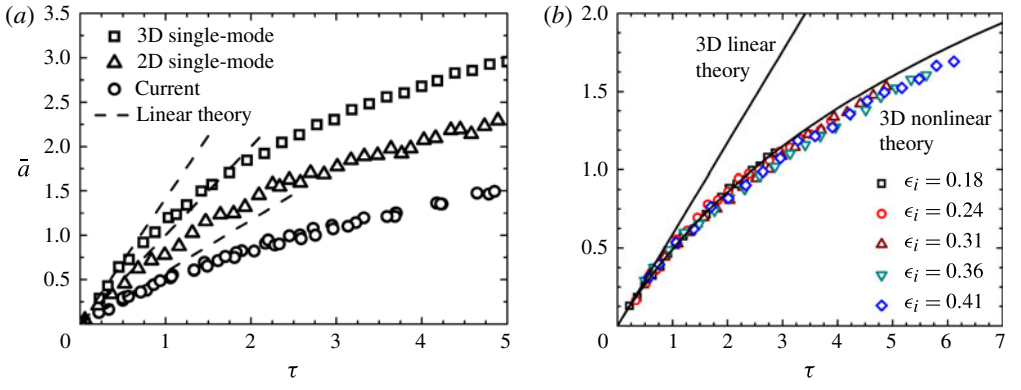


FIGURE 5. The dimensionless growth of the overall amplitude in the symmetry plane in comparison with (*a*) experimental results of the 3D single-mode (Chapman & Jacobs 2006) and 2D single-mode (Niederhaus & Jacobs 2003) and with (*b*) the theoretical models. $\epsilon_i = ka_i^0$.

amplitude, the stronger the baroclinic vorticity on the interface and the stronger the Mach reflection at the corner and, therefore, the faster the interfacial evolution.

4. Three-dimensional stability analysis in the symmetry plane

The growth in the present situation is quite different from the 2D case even at the linear stage as shown by the quantitative comparison in figure 5(*a*). In order to describe this behaviour, the 2D model (Mikaelian 2005), which predicts the RMI growth with an arbitrary initial interface, will be extended to the 3D situation.

The analysis considers a shock wave propagating along the z-axis impacting a flat interface (in the xy plane) with perturbations. We first define the initial perturbation on the interface with an arbitrary shape as

$$\eta(x, y, t_0) = \sum_{m,n} a_{mn} \cos(mk_x x + \varphi_{mx}) \cos(nk_y y + \varphi_{ny}), \tag{4.1}$$

where k_x and k_y are wavenumbers in the x- and y-directions, respectively, and t_0 the initial time. At the linear stage of the 3D RMI, we have

$$\eta(x, y, t) = \eta(x, y, t_0) + A^+ \Delta v F(x, y)(t - t_0), \tag{4.2}$$

where

$$F(x, y) = \sum_{m,n} a_{mn} \sqrt{(mk_x)^2 + (nk_y)^2} \cos(mk_x x + \varphi_{mx}) \cos(nk_y y + \varphi_{ny}). \tag{4.3}$$

In general, the extended model, i.e. (4.2), covers all the situations at their linear stages. In the 2D problem, the wavenumber k_y is zero and (4.2) reduces to the same form as that proposed by Mikaelian (2005). In the 3D single-mode RMI case, the interface can be described as $\eta(x, y, t_0) = a_{11} \cos(k_x x) \cos(k_y y)$ and (4.2) becomes

$$\eta(x, y, t) = \left[1 + \sqrt{{k_x}^2 + {k_y}^2} A^+ \Delta V (t - t_0)\right] a_{11} \cos(k_x x) \cos(k_y y), \tag{4.4}$$

https://doi.org/10.1017/jfm.2013.148 Published online by Cambridge University Press

where $k_x = k_y$. In the present 3D configuration, the geometry of the post-shock interface can be described as a multiple harmonic form based on (2.3),

$$\eta(x, y, t_0) = a_i^0 Z_c[2 - \cos(k_y y)]\cos(k_x x) + O\,(k_y y)^4, \tag{4.5}$$

where $k_x = k_y = k$. At the thin layer of the symmetry plane, the specific form of (4.3) is

$$F(x, y) = a_i^0 Z_c \left[2k_x - \sqrt{k_x^2 + k_y^2}\cos(k_y y)\right]\cos(k_x x). \tag{4.6}$$

Therefore, at the linear stage, the overall growth of the perturbations in the symmetry plane can be determined as

$$a_i^t = Z_c a_i \left[1 + \left(2k_x - \sqrt{k_x^2 + k_y^2}\right) A^+ \Delta V (t - t_0)\right]. \tag{4.7}$$

It is indicated that the predicted growth rate of the symmetry plane is $(2 - \sqrt{2})Z_c k a_i A^+ \Delta V$, which is 40 % slower than that of the 2D impulsive model. It should be noted that the curvature effect is reflected in the specific form of F. In the 3D single-mode case, the principal curvatures at the crest $(0, 0, a_{11})$ are $R_1^{-1} = R_2^{-1} = -k_x^2 a_{11}$. In the minimum-surface case, however, the principal curvatures are opposite at point $(0, 0, a_i)$, i.e. $R_1^{-1} = -k_x^2 a_i Z_c$ and $R_2^{-1} = k_y^2 a_i Z_c$.

Figure 5(*a*) compares the experimental results among the current, the 2D and 3D single-mode configurations (Niederhaus & Jacobs 2003; Chapman & Jacobs 2006). It can be seen that the extended linear theory (equation (4.2)) agrees well with the experiments at the early stage. Figure 5(*b*) shows a comparison of the experimental results in the present configuration with the theoretical models in their dimensionless forms. The quantities are non-dimensionalized as $\bar{a} = k(a_i^t - Z_c a_i^0)$ and $\tau = k v_i^{RM}(t - t_0)$. The experiments agree well with the extended 3D linear theory (equation (4.7)) up to $\tau = 0.7$. At the later time, the linear theory over-predicts the growth rate for all the cases because the nonlinearity becomes significant with the appearances of the bubble and spike. This asymmetric behaviour was extensively studied for the 2D RMI and the 3D single-mode RMI, and it was found that the growth rate of the instability decreases with time in the late evolution. However, there is a scarcity of results for the present 3D RMI. Inspired by previous studies on the 2D and 3D single-mode RMI (Sadot *et al.* 1998; Abarzhi 2001; Oron *et al.* 2001), the asymptotic growth rate of the current 3D RMI is assumed to be dependent on $1/(kt)$. An empirical model (Mikaelian 2003) that combines the early linear growth with the late-time nonlinear growth (Oron *et al.* 2001), is proposed:

$$v = \frac{v_0}{1 + k v_0 (t - t_0)/C}, \tag{4.8}$$

where v_0 is the growth rate at the linear stage and varies with the geometry of the shocked interface, i.e. (4.2), as $t \to t_0$, $v/v_0 \to 1$ and as $t \to \infty$, $v/v_0 \to C/(k v_0 t)$. The growth can be obtained by integrating (4.8),

$$a = a_0 + \frac{C}{k}\ln\left(1 + \frac{k v_0 (t - t_0)}{C}\right), \tag{4.9}$$

where a_0 is the post-shock amplitude. The experimental results show a good agreement with the 3D nonlinear theory when $C = 2A^+$, as illustrated in figure 5(*b*).

https://doi.org/10.1017/jfm.2013.148 Published online by Cambridge University Press

5. Conclusions

A method to generate a discontinuous gaseous interface in a well-controlled shape has been developed for a 3D RMI study. The interface formed has a minimum-surface feature and is free of support. Sequences of shocked air/SF_6 interfaces were recorded in shock-tube experiments by schlieren and planar Mie-scattering photography.

The instability evolution in the present configuration appears quite different from other 2D and 3D single-mode cases. At the linear stage the instability in the symmetry plane grows much slower than the predictions of previous 2D impulsive models. This is ascribed to the opposite principal curvatures of the minimum surface. The growth of perturbations tends to be suppressed by the opposite pressure gradient and baroclinic vorticity induced by the opposite principal curvature. The 2D impulsive model is extended to describe general 3D RMI. A quantitative analysis reveals a good agreement between experiments and the extended linear model for all the configurations including both the 2D and 3D RMIs at their early stages. Based on the asymptotic solution of the 3D RMI, an empirical model is also proposed to describe the whole evolution process of the symmetry plane from the early linear stage to the late-time nonlinear stage.

Our results provide both experimental evidence and a theoretical analysis of the effect of the second curvature on the 3D RMI, especially the opposite curvatures of the interface suppressing the growth of the instability. This may be useful for inertial confinement fusion target design.

Acknowledgements

This research is supported by the National Natural Science Foundation of China (Nos. 10972214 and 11272308). The authors would like to thank Mr M. Chen, Mr M. Wang and Dr Z. Zhai for their valuable help during the experiments.

References

ABARZHI, S. I. 2001 Asymptotic behaviour of three-dimensional bubbles in the Richtmyer–Meshkov instability. *Phys. Fluids* **13**, 2866–2875.

BROUILLETTE, M. 2002 The Richtmyer–Meshkov instability. *Annu. Rev. Fluid Mech.* **34**, 445–468.

CHAPMAN, P. R. & JACOBS, J. W. 2006 Experiments on the three-dimensional incompressible Richtmyer–Meshkov instability. *Phys. Fluids* **18**, 074101.

COLLINS, B. D. & JACOBS, J. W. 2002 PLIF flow visualization and measurements of the Richtmyer–Meshkov instability of an air/SF_6 interface. *J. Fluid Mech.* **464**, 113–136.

HAAS, J. F. & STURTEVANT, B. 1987 Interaction of weak shock waves with cylindrical and spherical gas inhomogeneities. *J. Fluid Mech.* **181**, 41–76.

ISENBERG, C. 1992 *The Science of Soap Films and Soap Bubbles*. Dover.

KRECHETNIKOV, R. 2009 Rayleigh–Taylor and Richtmyer–Meshkov instabilities of flat and curved interfaces. *J. Fluid Mech.* **625**, 387–410.

LAYES, G., JOURDAN, G. & HOUAS, L. 2009 Experimental study on a plane shock wave accelerating a gas bubble. *Phys. Fluids* **21**, 074102.

LEINOV, E., MALAMUD, G., ELBAZ, Y., LEVIN, L. A., BEN-DOR, G., SHVARTS, D. & SADOT, O. 2009 Experimental and numerical investigation of the Richtmyer–Meshkov instability under re-shock conditions. *J. Fluid Mech.* **626**, 449–475.

LONG, C. C., KRIVETS, V. V., GREENOUGH, J. A. & JACOBS, J. W. 2009 Shock tube experiments and numerical simulation of the single-mode, three-dimensional Richtmyer–Meshkov instability. *Phys. Fluids* **21**, 114104.

https://doi.org/10.1017/jfm.2013.148 Published online by Cambridge University Press

MARIANI, C., VANDENBOOMGAERDE, M., JOURDAN, G., SOUFFLAND, D. & HOUAS, L. 2008 Investigation of the Richtmyer–Meshkov instability with stereolithographed interfaces. *Phys. Rev. Lett.* **100**, 254503.

MESHKOV, E. E. 1969 Instability of the interface of two gases accelerated by a shock wave. *Fluid Dyn.* **4**, 101–104.

MIKAELIAN, K. O. 2003 Explicit expressions for the evolution of single-mode Rayleigh–Taylor and Richtmyer–Meshkov instabilities at arbitrary Atwood numbers. *Phys. Rev.* E **67**, 026319.

MIKAELIAN, K. O. 2005 Richtmyer–Meshkov instability of arbitrary shapes. *Phys. Fluids* **17**, 034101.

NIEDERHAUS, C. E. & JACOBS, J. W. 2003 Experimental study of the Richtmyer–Meshkov instability of incompressible fluids. *J. Fluid Mech.* **485**, 243–277.

ORON, D., ARAZI, L., KARTOON, D., RIKANATI, A., ALON, U. & SHVARTS, D. 2001 Dimensionality dependence of the Rayleigh–Taylor and Richtmyer–Meshkov instability late-time scaling laws. *Phys. Plasmas* **8**, 2883–2889.

RANJAN, D., OAKLEY, J. & BONAZZA, R. 2011 Shock-bubble interactions. *Annu. Rev. Fluid Mech.* **43**, 117–140.

RICHTMYER, R. D. 1960 Taylor instability in shock acceleration of compressible fluids. *Commun. Pure Appl. Maths* **13**, 297–319.

RIKANATI, A., ORON, D., SADOT, O. & SHVARTS, D. 2003 High initial amplitude and high Mach number effects on the evolution of the single-mode Richtmyer–Meshkov instability. *Phys. Rev.* E **67**, 026307.

SADOT, O., EREZ, L., ALON, U., ORON, D., LEVIN, L. A., EREZ, G., BEN-DOR, G. & SHVARTS, D. 1998 Study of nonlinear evolution of single-mode and two-bubble interaction under Richtmyer–Meshkov instability. *Phys. Rev. Lett.* **80**, 1654–1657.

SI, T., ZHAI, Z., YANG, J. & LUO, X. 2012 Experimental investigation of reshocked spherical gas interfaces. *Phys. Fluids* **24**, 054101.

WANG, M., SI, T. & LUO, X. 2013 Generation of polygonal gas interfaces by soap film for Richtmyer–Meshkov instability study. *Exp. Fluids* **54**, 1427.

YOSEF-HAI, A., SADOT, O., KARTOON, D., ORON, D., LEVIN, L. A., SARID, E., ELBAZ, Y., BEN-DOR, G. & SHVARTS, D. 2003 Late-time growth of the Richtmyer–Meshkov instability for different Atwood numbers and different dimensionalities. *Laser Part. Beams* **21**, 363–368.

ZABUSKY, N. J. 1999 Vortex paradigm for accelerated inhomogeneous flows: visiometrics for the Rayleigh–Taylor and Richtmyer–Meshkov environments. *Annu. Rev. Fluid Mech.* **31**, 495–536.

ZHAI, Z., SI, T., LUO, X. & YANG, J. 2011 On the evolution of spherical gas interfaces accelerated by a planar shock wave. *Phys. Fluids* **23**, 084104.

ZHANG, Q. & SOHN, S. I. 1999 Quantitative theory of Richtmyer–Meshkov instability in three dimensions. *Z. Angew. Math. Phys.* **50**, 1–46.

https://doi.org/10.1017/jfm.2013.148 Published online by Cambridge University Press